ACS APPLIED MATERIALS & INTERFACES

Research Article

www.acsami.org

Nanocrystalline Brookite with Enhanced Stability and Photocatalytic Activity: Influence of Lanthanum(III) Doping

Céline Perego,[†] Yu-heng Wang,[‡,§,⊥] Olivier Durupthy,*[,‡,§,⊥] Sophie Cassaignon,[‡,§,⊥] Renaud Revel,[†] and Jean-Pierre Jolivet[‡,§,⊥]

[†]IFP Energies nouvelles, Rond point de l'échangeur de Solaize, BP 3, 69360 Solaize, France

[‡]UPMC Univ Paris 06, UMR 7574, Chimie de la Matière Condensée de Paris, [§]CNRS, UMR 7574, Chimie de la Matière Condensée de Paris, and [⊥]Chaire de Matériaux Hybrides, UMR 7574, Collège de France, 11 place Marcelin Berthelot, 75231 Paris Cedex 05, France

Supporting Information

ABSTRACT: Metastable TiO_2 polymorphs are more promising materials than rutile for specific applications such as photocatalysis or catalysis support. This was clearly demonstrated for the anatase phase but still under consideration for brookite, which is difficult to obtain as pure phase. Moreover, the surface doping of anatase with lanthanum ions is known to both increase the thermal stability of the metastable phase and improve its photocatalytic activity. In this study, TiO_2 nanoparticles of almost only the brookite structure were prepared by a simple sol−gel procedure in aqueous solution. The nanoparticles were then doped with lanthanum(III) ions. The thermal stability of the nanoparticles was analyzed by X-ray diffraction and kinetic models were successfully applied to quantify phases evolutions. The presence of surface-sorbed lanthanum(III) ions increased the phase stability of at least 200 °C and this temperature shift was attributed to the selective phase stabilization of metastable TiO_2 polymorphs. Moreover, the combination of the surface doping ions and the thermal treatment induces the vanishing of the secondary anatase phase, and the photocatalytic tests on the doped brookite nanoparticles demonstrated that the doping increased photocatalytic activity and that the extent depended on the duration of the sintering treatment.

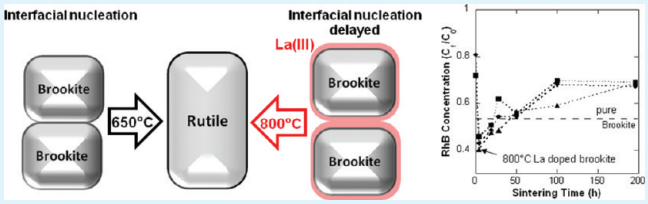

KEYWORDS: *titanium dioxide, brookite, phase transformation, lanthanum, sintering, kinetic parameters, photocatalysis*

1. INTRODUCTION

Research on TiO_2 powder synthesis is of great interest thanks to its numerous applications such as pigment, UV blocker, photocatalyst, electrochromic material, oxygen sensor, lithium-ion battery, and dye-sensitized solar cell (DSSC).[1−8] The efficiency of the oxide in each of those applications depends on the phase, size, and shape of the particles used. Indeed, it is commonly recognized that the anatase polymorph displays higher photoactivity than brookite or rutile.[9] However, for that specific application, recent studies demonstrated that the use of brookite polymorph, as a pure phase or combined with anatase or rutile, is almost as good as anatase;[10−18] Indeed the phase mixture involving anatase and brookite recall the commercial TiO_2 P25 (Evonik) which is also a phase mixture (80% of anatase and 20% rutile). To improve the photoactivity, an increase in crystallinity through a thermal treatment is often performed but the counterparts are an important loss in specific surface over 400 °C and a phase transition to the thermodynamically stable rutile polymorph at higher temperatures. Indeed, the two metastable TiO_2 polymorphs, anatase and brookite are converted into rutile at high temperature.[19,20] A huge amount of studies are devoted to the tailoring of TiO_2 nanoparticles in term of structure, size and shape[21−27] but few is interested in the way by which these characteristics are modified in the purpose that the particles are converted into a really functional material. That is why the study of the evolution of TiO_2 nanopowders in function of temperature of sintering treatment is mandatory for each polymorph.

The anatase to rutile phase transformation has been widely studied over the last twenty years, and various kinetic models have been proposed.[28−38] Anatase particles size and shape were shown to impact the stability of the polymorph.[39−42] Moreover, the deposition on anatase particles of metal ions such as Al^{3+}, Ca^{2+}, or La^{3+} at a relatively low surface concentration was shown to significantly improve the thermal stability of that polymorph.[41,43−46] The choice of doping ions is of paramount importance, because it may enhance or poison the foreseen property. In the case of photocatalysis applications, anatase particles covered with lanthanum seem to display enhanced properties.[46]

Unlike the anatase, fewer studies were reported on the phase transformation of the brookite polymorph.[38,47−51] This is

Received: October 11, 2011
Accepted: December 27, 2011
Published: December 27, 2011

probably due to the fact that efficient pathways to yield large amounts of pure brookite emerged only recently.[52−54] Moreover, natural brookite contains usually high amount of impurities.[47,49] Sintering of synthetic brookite nanoparticles was already described but, to the best of our knowledge, only one group studied the surface doping of brookite for improved thermal stability or enhanced photocatalytic activity[55,56] and few studies are devoted to the activity of TiO_2 mixtures involving brookite as major phase.[10,12,13,17]

In this context, we present in this study a detailed description of lanthanum doped brookite nanoparticles phase transformation. One of the main objectives is to determine whether the influence of lanthanum on the thermal stability and photocatalytic activity of the anatase polymorph might be transposed to brookite. Therefore, we synthesized TiO_2 nanoparticles with brookite as the majority phase (> 95%) using sol-gel methods. The powders were impregnated with lanthanum ions and sintered at various temperatures. Their size evolution and their kinetics of phase transformation in function of sintering treatment were studied using mainly X-ray diffraction (XRD). Specific attention was paid to the presence of a secondary anatase phase using Raman spectroscopy. In certain conditions, the kinetic models developed for the anatase phase transformation could be transposed to the doped brookite system, whereas in other cases, new sintering scenarios, which take into account the formation of a lanthanum titanium mixed oxide phase, were proposed. Moreover, we studied the photocatalytic degradation of Rhodamine B under UV light in order to compare the photocatalytic activity of the doped material thermally treated for different durations to the nondoped and nonheated reference sample of brookite.

2. EXPERIMENTAL SECTION

2.1. Particles Synthesis. The brookite particles were obtained through the co-thermohydrolysis at 60 °C of the aqueous precursors $TiCl_3$ and $TiCl_4$.[20] An equimolar solution of Ti^{3+} and Ti^{4+} (0.1 mol L^{-1}) was prepared and the pH was adjusted to 4.5 with NaOH solution of 5 mol L^{-1}. The suspension was aged one week at 60 °C without stirring. The particles were flocculated by increasing the pH up to 6 with NaOH (close to the isoelectric point[57]). Then the precipitates were collected by filtration of the colloidal suspension. and washed several times with deionized water. Powders were finally dried under air at 100 °C.

2.2. Particle Impregnation. A concentrated suspension of TiO_2 particles is obtained by pouring under vigorous stirring dry powder in distillated water up to a weight concentration of 20 g L^{-1}. The pH of the colloidal solution was set to 7 with ammonia. A stock solution of La^{3+} ions at a concentration of 0.35 mol·L^{-1} was prepared by the dissolution of solid lanthanum nitrate ($La(NO_3)_3$. $6H_2O$). Defined amounts of the La^{3+} solution are introduced in the TiO_2 dispersion. The pH was set back to 7 and the suspension was stirred during 2 h at room temperature. The powder is then collected by filtration and the supernatant solution is kept for analyses. A 'reference sample' was also prepared with the same impregnation process but with a lanthanum-free solution.

2.3. Sintering Procedures. The sintering of non impregnated samples and impregnated samples were first performed under a temperature ramp in order to determine the critical temperatures for a more precise study. The experiments were conducted by in situ X-ray diffraction, where the sample was heated at 5°.min^{-1} from 100 °C up to 900 °C, under an air flow, with 50 °C steps at which an X-ray diffractogram was collected. Kinetic experiments at a constant temperature (800 or 900 °C) were performed according two different methods depending on the speed of the phase transformation. The 800 °C sintering experiments were performed in a furnace. Few grams of each impregnated sample were put in alumina crucibles, first heated at a heating rate of 5° min^{-1} up to 250 °C for a 2 h pretreatment (designed to remove most surface physisorbed water and organic leftover) and finally raised to the desired sintering temperature of 800 °C. The samples were taken out of the furnace and quenched, to avoid the impact of a slow decrease of temperature. The transformations take place much faster at 900 °C and therefore experiments were conducted by in situ X-ray diffraction, where the sample was heated according to the same temperature ramp to the target temperature. X-ray data were collected every 20 min all along the sintering time.

2.4. Characterization. The structure and size of the nanoparticles were determined using a precise deconvolution of the corresponding X-ray diffraction (XRD) patterns. Bragg−Brentano XRD measurements were performed on a Panalytical X'Pert Pro diffractometer using filtered Cu K_α radiation over a 2θ range from 5° to 80° with a step size of 0.033° and a counting time of 300 s per step. In situ Bragg−Brentano XRD measurements were carried out in an Anton Paar XRK900 cell using a PANalytical X'Pert Pro diffractometer equipped with a position sensitive detector (X'Celerator). Patterns were analyzed using the Diffrac Plus Evaluation software from Bruker. At least three lines of the diffraction patterns were chosen for each polymorph for the crystal size estimation. The size of the particles in a defined direction, D_{hkl}, was calculated by applying the Scherrer formula, $D_{hkl} = 0.9\lambda/B_{hkl} \cos\theta$, to the line width at half-maximum, B_{hkl}, corrected for the instrument broadening assuming a Gaussian profile. It was also assumed that line broadening is mainly due to the particle size effect. Particles were considered as spherical in the present study and the crystal size was defined as the mean value of the dimensions in the different directions. The approximate proportions of the different TiO_2 polymorphs, anatase, brookite, and rutile, in the solids were evaluated from the relative areas of the rutile [110] (d = 3.247 Å), brookite [121] (d = 2.898 Å), and anatase [101] (d = 3.509 Å) diffraction lines. The calibration parameters were determined according to a previous study and the determination of incertitude on phase fractions gave ±2 %.[24] However, when an additional crystalline phase was observed, its contribution was not taken into account in the phase distribution and the evolution of its concentration in the solid could only be qualitatively estimated.

High-resolution transmission electron micrographs (HR-TEM) and selected area electron diffraction (SAED) were performed either on a FEI Tecnai 20F Ultratwin instrument at an acceleration voltage of 200.0 kV or on a FEI Tecnai Spirit G2 instrument at an acceleration voltage of 120.0 kV. The d-spacings obtained from the SAED pattern were calibrated using Au pattern. The nanoparticles were ultrasonicated in water and dispersed on carbon covered Cu-grids.

The Raman spectra were recorded in the range 100 to 3450 cm^{-1} on a commercial modular Raman spectrometer (Raman Analyzer RXN1 microprobe of Kaiser Optical Systems, Inc.). It displays a high-powered near-IR laser diode working at 785 nm that minimizes possible strong fluorescence from lanthanum.

The N_2 sorption studies and specific surface area measurements were carried out at 77 K using a Micromeritics ASAP 2000 instrument. The BET method was applied to determine the specific surface area.

Lanthanum(III) concentration in supernatant solution was determined by UV−visible spectroscopy measurements of a coloured complex formed with the arsenazo III molecules as described in the literature.[58]

2.5. Photocatalytic Activity Test. Experiments of rhodamine B (RhB) degradation were conducted in a suspension containing nanoparticles under ultraviolet illumination. The experiments were carried out in a 200 mL glass beaker, and the ultraviolet illumination was provided from the top of the reactor by a Philips Cleo performance 40W without filtration. A RhB stock solution with an absorbance of 2 at a wavelength of 555 nm was prepared. Certain amount of TiO_2 sample were dispersed in 100 mL of RhB solution by magnetic stirrer for 20 minutes in the dark, in order to homogenize the reactive system and to reach the adsorption−desorption equilibrium. The medium was then illuminated with the UV lamp. The quantity of different samples used was decided in such a way ("iso-surface") that the surface areas of added samples were all equal to 10 m^2. The

suspension was illuminated during 2 h, followed by centrifugation, and the RhB concentration in the supernatant was then analyzed by measuring absorption at the wavelength of 555 nm with a UV−visible spectrophotometer UVIKON XL from SECOMAN. The photocatalytic activity can thus be negatively correlated to the concentration of remaining RhB.

3. RESULTS AND DISCUSSION

3.1. Characterization of the Undoped TiO_2 Nanoparticles. The described synthesis yields almost pure phase brookite nanoparticles and only a careful study of the XRD and Raman analyses confirm the presence of very few amounts of anatase (estimated to less than 5%). Indeed, in the diffractogram displayed in Figure 1a all the peaks could be attributed to

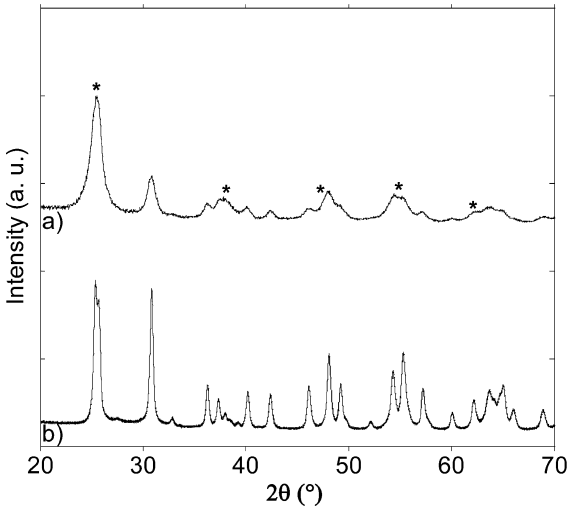

Figure 1. X-ray diffraction patterns of (a) the reference sample and (b) 1.0 at.nm-2 La covered brookite nanoparticles sintered 4h at 800 °C. The diffractograms were indexed according to the 29-1360 JCPDS file. The * correspond to the main anatase peaks positions.

brookite (PDF 00-29-1360). However, as most of the peaks corresponding to anatase (PDF 00-21-1272) are beneath those of brookite, more attention should be paid to the relative intensity of each peak. For instance, the intensity ratio between the (210) and (111) peaks around 2θ = 25.26 and 25.71° and the peak corresponding to the (211) plane at 2θ = 30.83° is expected to be close to 1 while here it is more than two. Moreover the intensity of the peak around 2θ = 38° is too intense to be only due to brookite peaks and may be explained by the presence of the (004) peak of anatase (2θ = 37.80°). The Raman peaks of the two polymorphs are significantly different as reported in figure 2. According to the group theory, four modes are Raman active in the brookite structure resulting in 15 vibration bands in the 100 to 700 cm^{-1} range which are A_{1g} (155, 194, 247, 412, and 636 cm^{-1}), B_{1g} (213, 322, and 501 cm^{-1}), B_{2g} (366, 395,460 and 583 cm^{-1}) and B_{3g} (172, 287, and 545 cm^{-1}).[59] As for anatase only six bands are reported in the same wave number range corresponding to the six Raman active vibration modes: 144 cm^{-1} ($E_g(1)$), 197 cm^{-1} ($E_g(2)$), 399 cm^{-1} ($B_{1g}(1)$), 513 cm^{-1} (A_{1g}), 519 cm^{-1} ($B_{1g}(2)$) and 639 cm^{-1} ($E_g(3)$).[60] The Raman spectrum of as prepared TiO_2 nanoparticles clearly display the peaks corresponding to the brookite structure but two additional small peaks are observed at 397 and 512 cm^{-1} indicating the presence of small amounts of anatase.

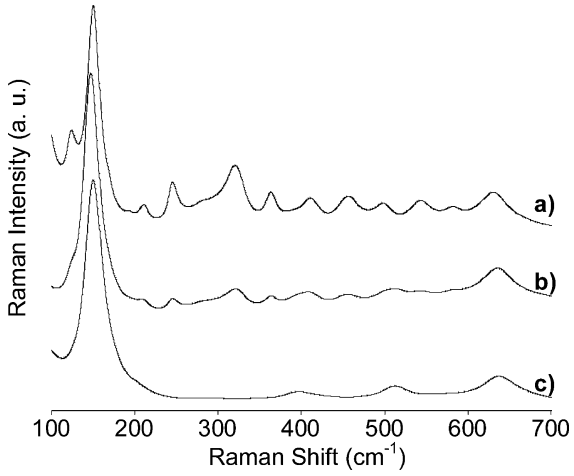

Figure 2. Raman spectra of (a) reference brookite particles, (b) as-prepared brookite sample, and (c) reference anatase particles.

The precise size and morphology of brookite and anatase nanoparticles in the reference sample could not be estimated from the XRD pattern and the Scherrer formula because of the overlapping of the peaks corresponding to the two structures. The transmission electron micrograph displayed in Figure 3a and 3c show brookite nanoparticles with rice like shape of about 15 nm long and 10 nm width. The observed fringes correspond to (210) or (111) lattice planes. The size and shape of the anatase particles may not be very different from those of brookite and the characteristic (101) fringes of the anatase particles are close those of brookite. That is why it is hard to distinguish one from another. However, in some anatase particles, the (101) fringes intersect with a defined angle. This peculiar feature was not observed in the different micrographs indicating that the amount of anatase in the sample must be very low. The SAED micrograph on a large domain of the grid reported in Figure 3b and its 1D projection confirm that the observed particles are overwhelmingly brookite. The as-synthesized brookite nanoparticles display a relatively high specific surface area of 175 m^2 g^{-1} and about 170 ppm of sodium impurities (probably from the sodium hydroxide used at the flocculation step).

3.2. Lanthanum-Doped Brookite Nanoparticles. Titanium dioxide nanoparticles were impregnated with lanthanum-(III) ions in order to increase their thermal stability. First, lanthanum adsorption isotherms were experimentally determined on brookite nanoparticles and are reported in the Supporting Information, S1. Then, three expected surface coverage (0.4, 0.7, and 1 at nm^{-2}, or 0.66, 1.16, and 166 μmol/m^2) were selected for sintering experiments according to previous studies on anatase demonstrating that significant effects are observed for surface coverage in the range of 0.3 to 1.6 at nm^{-2}.[46,61] The XRD patterns of the doped sample reported in the Supporting Information, S2, do not significantly differ from that of the reference sample.

The influence of surface lanthanum ions on titanium dioxide thermal stability was first confirmed with a dynamic study. The amount of rutile obtained with temperature and the particles mean size of the different polymorphs are reported in Figure 4. Interestingly, in the diffractograms of the sintered materials, the ratio between the peaks at 25.26 and 30.83° was found to be close to 1 indicating that the samples does not contain anatase any more (cf. figure 1b), which is also demonstrated later in the

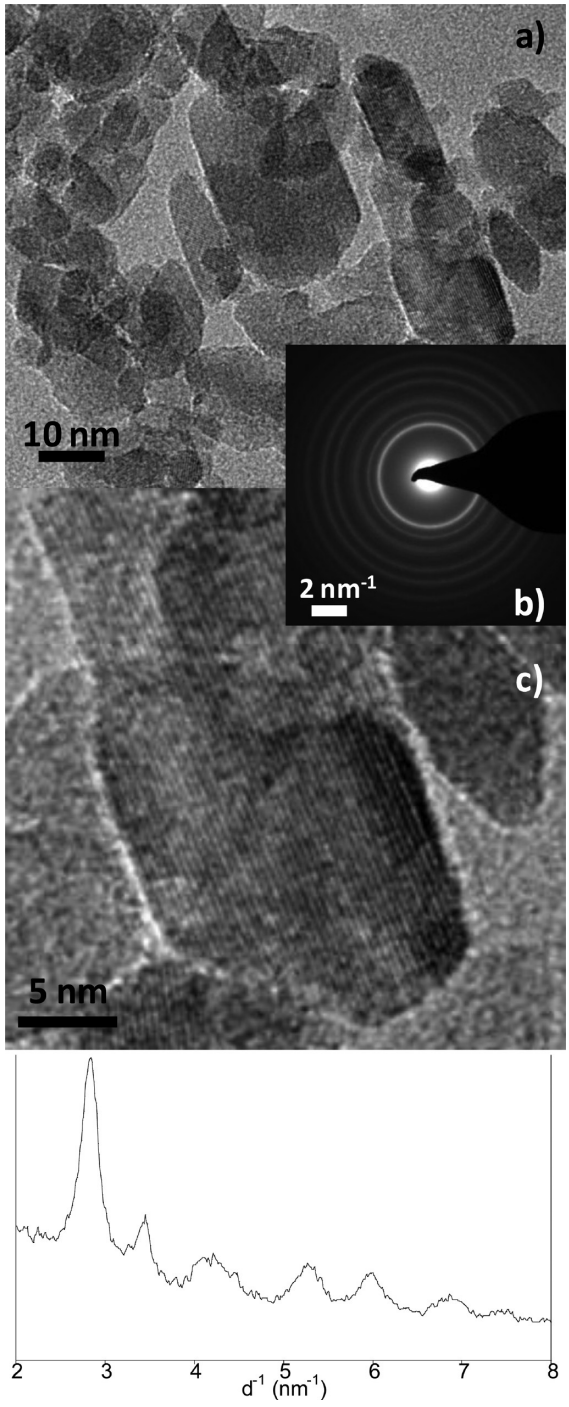

Figure 3. (a, c) Electron micrographs of as-synthesized brookite nanoparticles, (b) SAED micrograph representative of the whole sample. The additional diagram corresponds to a radial measure of the intensity of the SAED image. Observed fringes on c correspond to (210) or (111) planes on brookite nanoparticles.

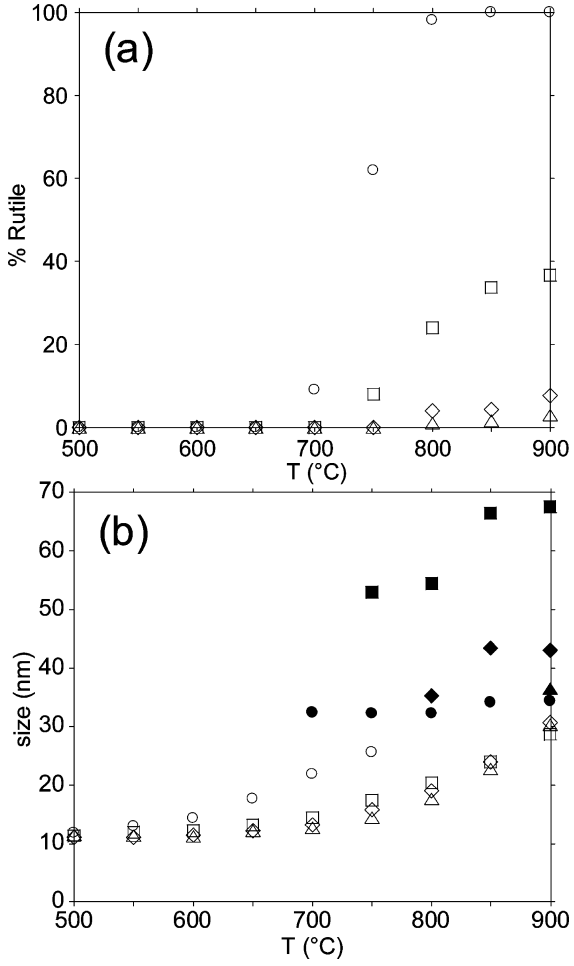

Figure 4. Sintering of La(III)-doped brookite nanoparticles: (a) amount of rutile formed with temperature from undoped brookite (○), brookite doped with La(III) at 0.4 at nm^{-2} (□), 0.7 at nm^{-2} (◇), and 1.0 at nm^{-2} (Δ); (b) corresponding particles size of brookite (empty dots ○, □, and ◇) and rutile (plain dots ■,◆, and●).

constant temperature experiments with Raman spectroscopy (cf. also the Supporting Information, S3). Moreover, the formation of the rutile particles is clearly delayed to higher temperature with lanthanum doping. Indeed, transformation of brookite to rutile starts around 650 °C in undoped brookite particles and 750−800 °C for doped ones. At 800 °C, the transformation is almost complete for undoped TiO_2, whereas it is limited to a maximum of 40% for doped materials. This suggests that lanthanum is an efficient surface stabilizer of metastable TiO_2 polymorphs. The observed trend is very similar to that observed with samarium(III), where 1% doping is enough to increase the transformation temperature of more than 50 °C.[55,56] The delay in phase transition might be explained by the fact that the surface impregnated particles display Ti−O−La terminations that stabilize the surface energy.[56] Consequently the particles start to grow at higher temperatures and reach critical size for phase transition later.[37] Another possible explanation proposed in the literature is that the presence of the dopant changes the defect structure of TiO_2 or the amount of oxygen vacancies.[46,62] The mean size of formed rutile particles also depends on the surface doping since larger particles are obtained in the presence of lanthanum. All these results suggest that the surface lanthanum ions infer on phase transformation mechanisms.

To provide new insights in the brookite to rutile transformation mechanisms, we sintered lanthanum-doped samples at constant temperatures of 800 or 900 °C. Experimental data of rutile amount with time and evolution of particles mean size for the ex-situ experiments at 800 °C are reported in the Supporting Information, S4. These kinetics data were fit with different models usually used for anatase to rutile transformation and that are displayed in Table 1. The models that are able to fit correctly the data are the models developed by

dx.doi.org/10.1021/am201397n | ACS Appl. Mater. Interfaces 2012, 4, 752−760

Table 1. Kinetic Models Describing Phase Transformation of Anatase to Rutile

kinetics models references	equation[a]
1. standard 1st order [71−73]	$\ln(1-\alpha) = -kt$
2. standard 2nd order[74]	$(1-\alpha)^{-1} - 1 = kt$
3. contracting spherical interface[62,75,76]	$(1-\alpha)^{1/3} = kt + c$
4. nucleation and growth of overlapping nuclei[62,75]	$[-\ln(1-\alpha)]^{1/3} = kt$
5. one-dimensional, linear, branching nuclei and constant growth [62,75]	$\ln \alpha = kt + c$
6. random nucleation and rapid growth [62,75]	$\ln(1-\alpha) = kt + c$
7. JMAK model [77−80]	$\ln[-\ln(1-\alpha)] = n\ln k + n\ln t$
8. interface nucleation and constant nuclei growth (INCNG)[36]	$1/((1-\alpha)(D_0/D)^3) - 1 = k_2 t^{(m-1)/m}$
9. pure interface nucleation (IN)[64]	$(D_0/D)^3/(1-\alpha) - 1 = (k_2 N_0)t$
10. combined interface and surface nucleation (CISN)[64]	$(D_0/D)^3/(1-\alpha) - 1 = (1 + (k_2 N_0/k_1))(e^{k_1 t} - 1)$

[a] α = fraction of transformation, t = time, k = kinetic constant, D = mean particle size, D_0 = initial particle size, n = Avrami exponent, m = an exponent describing the grain growth behavior,[70] and N_0 = initial number of particles.

Banfield et al.[63] that take the particles size into account. The main difference between the different mechanisms proposed by Banfield is the place where the phase transformation is initiated: at the interface between two particles (interface nucleation or IN), at the surface of single particle (surface nucleation or SN) or in the bulk of the nanoparticle (bulk nucleation or BN). The energies needed to nucleate the new phase on these different sites increase from the interface to the bulk but the amount of the corresponding nucleation site evolves in the other way. Consequently, in the anatase to rutile transformation system, the observed mechanism evolves from IN to SN and finally BN with increasing temperature. Moreover, the formation of the nuclei is supposed to be the kinetically limiting step but at low temperature the kinetics of the growth of the nuclei may infer on the global phase transformation kinetics and a model titled interface nucleation and constant growth of the nuclei (INCNG) was proposed. Among the described models, the best fit was obtained with the INCNG model as shown in figure 5. The corresponding values of k_2 and m (k_2 is a kinetic constant associated to the interfacial nucleation and m is an exponent related to the grain growth behavior) displayed in table 2 indicate that, for roughly the same value of the exponent m = 1.4, the kinetic constants are more than two times smaller with higher amounts of lanthanum: k_2 = 4.1 $h^{(1-m)/m}$ for 1.0 at nm^{-2} of La(III) compared to k_2 = 9.9 $h^{(1-m)/m}$ for 0.4 at nm^{-2} of La(III). Those data are compared to those previously published on undoped particles[20] and it was found that the calculated value of k_2 in the doped system at 800 °C are close to that obtained at 650 °C on undoped brookite particles with k_2 = 5.1 $h^{(1-m)/m}$ and m = 1.7.

The validity of the (INCNG) model (8 in Table 1) for sintering at significantly high temperature suggests that all the mechanisms that involve the surface such as pure interface nucleation (IN) model (9 in Table 1) and surface nucleation model[64] (SN) are delayed when TiO_2 is stabilized with lanthanum. The interaction of lanthanum with the oxide surface is consequently a key parameter of the TiO_2 metastable phase stabilization. Sibu et al. proposed that lanthanum is present at the surface of sintered TiO_2 particles rather as La_2O_3 small particles than as isolated ions.[65] However, only one previous study indicated the presence of very weak XRD peaks in doped

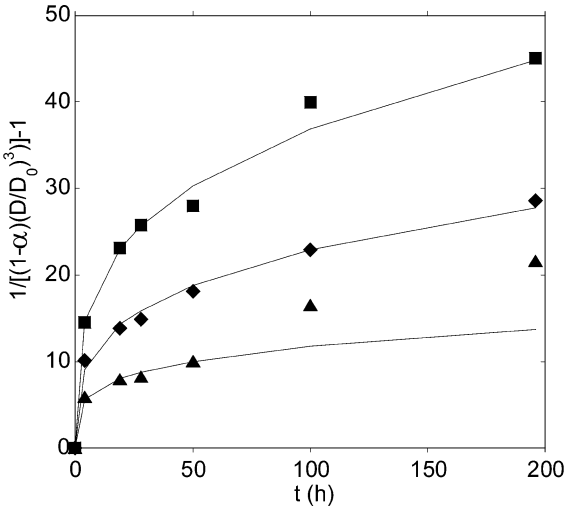

Figure 5. Experimental data of La(III)-doped brookite nanoparticles sintered at 800 °C fitted with the interface nucleation and growth of the nuclei model for a La(III) load of 0.4 at nm^{-2} (■), 0.7 at nm^{-2} (◆), and 1.0 at.nm^{-2} (▲). Plain lines correspond to the fit with the selected kinetic model.

Table 2. Kinetic Parameters of the Fit Obtained for Brookite Nanoparticles Doped with Different Loads of La and Various Sintering Conditions

exp. conditions	$[La^{3+}]$ (at nm^{-2})	k_2 ($h^{(1-m)/m}$)	m
600 °C/0−60 h	0	1.3	1.6
650 °C/0−60 h	0	5.1	1.7
700 °C/0−18 h	0	20.8	1.5
800 °C/0−200 h	0.4	9.9	1.4
800 °C/0−200 h	0.7	6.1	1.4
800 °C/0−50 h	1.0	4.1	1.3

materials confirming the presence of crystalline lanthanum oxide.[44] In the present study, no diffraction peaks indicating the presence of crystalline lanthanum oxide could be observed in the sintered samples. Meanwhile, the presence of an amorphous or poorly crystalline oxide phase containing lanthanum could not be excluded. Indeed, when examining closely the sintered particles with lanthanum at the very first hours of treatment with TEM, one can observe on Figure 6a an amorphous coating at the surface of the brookite particles. On the corresponding SAED micrograph displayed in Figure 6b, no diffraction rings beside those of brookite could be observed. XPS studies on La doped anatase provided in the literature[66−68] and results in our group (not shown) indicate that La is more likely present as an amorphous lanthanum oxide phase La_2O_3 rather than isolated La ions forming La−O−Ti bonds. An XPS signal corresponding to that kind of bonding was found in samarium doped samples[69] but never with lanthanum. This La_2O_3 layer could then act as a barrier between two brookite particles. Whatever the structure of lanthanum at the surface of TiO_2 nanoparticles, it clearly inhibits the phase transformation of brookite to rutile. For roughly amorphous lanthanum oxide, the m parameter in the INCGN model (8) is the same as that of undoped samples, indicating the same grain growth mechanism.[36,70] The phase transformation is then only slowed down by the presence of lanthanum at the interface between two particles that blocks the nucleation of rutile.

A crystalline mixed titanium and lanthanum oxide phase was evidenced in samples sintered at 900 °C (see the Supporting

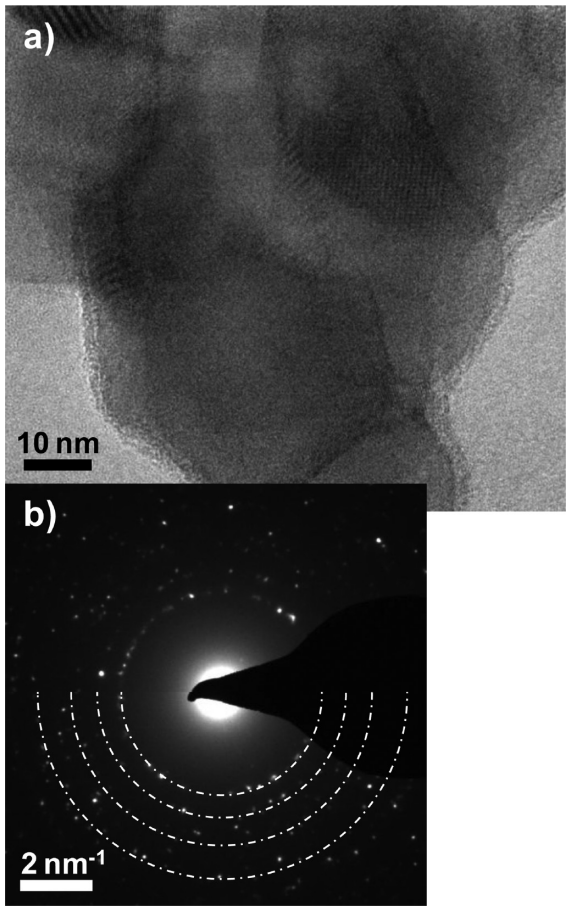

Figure 6. Electron micrographs of 1.0 at nm^{-2} La doped brookite nanoparticles sintered 4h at 800 °C (a) and SAED micrograph representative of the whole sample b). The additional semicircles correspond to the main distances for the SAED image of a pure multicrystalline brookite sample ((210)+(111), (211), (102)+(021), and (321)).

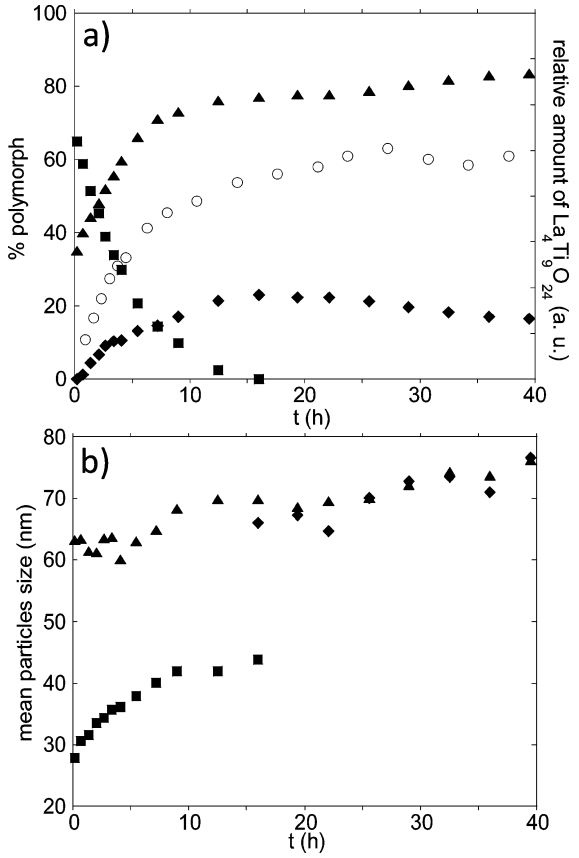

Figure 7. In situ sintering of 0.4 at nm^{-2} La-doped brookite nanoparticles at 900 °C: (a) evolution with time of the amount of brookite (■), anatase (◆), and rutile (▲) and (b) the corresponding particles size. In a, the qualitative amount of the additional $La_4Ti_9O_{24}$ structure is plotted with (○).

Scheme 1. Proposed Schematic Pathway for the La Impregnated Brookite Nanoparticles (Grey Rounds) Phase Transition into Anatase (White Rounds) and Rutile (Black Rounds) at 900 °C[a]

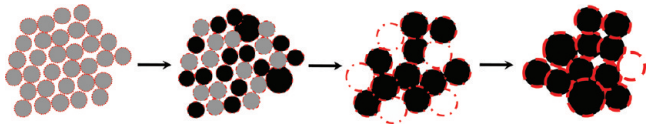

[a]Small red dots stand for homogeneously scattered islands of a La rich phase on TiO_2 and long segments stand for crystallized $La_4Ti_9O_{24}$.

Information, S5). An already described $La_4Ti_9O_{24}$ structure was observed in less than 2 h in all the doped samples.[44,68] The evolution of the mineralogical composition and the mean particle size for the sample with a lanthanum load of 0.4 at nm^{-2} is reported in figure 7. A qualitative evolution of the mixed lanthanum and titanium oxide is also plotted. Anatase was observed as a transitory phase and consequently the sintering of brookite at 900 °C could not be described using only one mechanistic model. The presence of the anatase phase may be related here to its presence in the pristine material, but at high lanthanum loading, the anatase phase first disappeared at the beginning of the thermal treatment and then appeared again after several hours (see the Supporting Information, S6). Moreover, the amount of anatase formed is significantly higher than the initially estimated 5% of anatase. A proposition of mechanistic scheme is given in Scheme 1. At room temperature and in the very first step of the sintering, brookite particles are uniformly covered with lanthanum ions (probably as an oxide) that prevents a rapid interfacial nucleation as discussed previously. Consequently, rutile may be obtained both by IN (model 9) or SN mechanisms.[64] The formation of rutile particles with the same size as the pristine brookite particles for high loads of lanthanum suggests that the SN mechanism is favored. After this first short period, lanthanum or titanium ions migrate at the interface of La_2O_3/TiO_2 to form the crystallized lanthanum titanium oxide phase and consequently parts of the nanoparticles surfaces may be free. IN mechanism for rutile may then takes place and significantly bigger rutile nanoparticles are formed. Anatase particles are also formed at the same stage of the sintering or slightly later for high loads of lanthanum and their size is also bigger than that of initial brookite particles. Finally, after all brookite is transformed into either rutile or anatase, the anatase particles covered with $La_4Ti_9O_{24}$ slowly converts into rutile through an IN or SN mechanism. The duration of each mechanistic step depends on the lanthanum loading. Indeed, for higher surface coverage, the complete transformation of brookite and the appearance of anatase are slower, whereas the formation of the $La_4Ti_9O_{24}$ phase is accelerated and enhanced. However, a same maximum anatase rate of 20% is observed whatever the surface coverage.

dx.doi.org/10.1021/am201397n | ACS Appl. Mater. Interfaces 2012, 4, 752−760

The final anatase to rutile transformation mechanism could not be clearly defined because the amount of anatase converted in the last 25 h of the sintering is too low to infer on the rutile particle size evolution when converted. The anatase is not observed as transitory phase until the formation of mixed lanthanum and titanium oxide phase. This might suggest that the mixed oxide phase is able to stabilize specifically anatase nanoparticles at very high temperature. However, with longer sintering, the metastable phase still transform into rutile at this temperature. More detailed comparisons between the three TiO_2 polymorphs and $La_4Ti_9O_{24}$ would be necessary to clearly demonstrate the different structures stabilization, but it is possible that the stacking of TiO_6 octahedra in anatase and in brookite is less regular than in rutile and consequently may fit more easily with the lanthanum-containing structure. To summarize the transformation, La-doped brookite first convert into rutile until the $La_4Ti_9O_{24}$ phase is formed at the surface, then, it converts into both anatase and rutile. Finally, when all the brookite vanished the anatase particles are converted into rutile. The proposed role of lanthane is to impact, depending on its structure at the titanium oxide surface, on the kinetics of different phases transformations B→A, B→R, and A→R.

3.3. Photocatalytic Activity Tests on Lanthanum-Doped Brookite Nanoparticles Sintered at 800 °C. The results of the photocatalytic activity tests are shown in Figure 8.

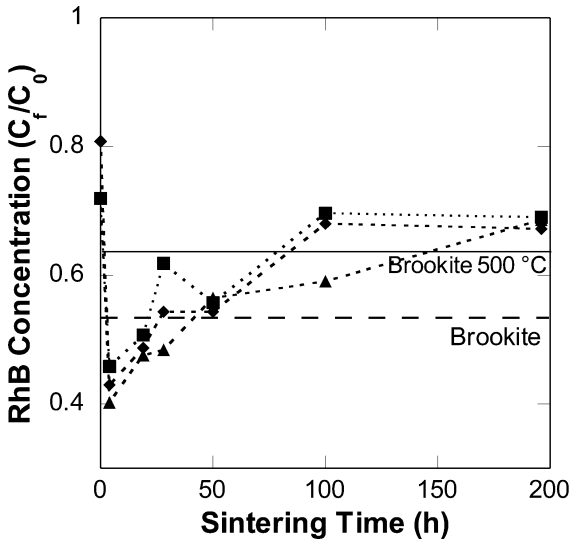

Figure 8. Photocatalytic activity test results of La(III)-doped brookite nanoparticles sintered at 800 °C as function of sintering time for a La(III) surface coverage of 0.4 at.nm^{-2} (■), 0.7 at nm^{-2} (◆) and 1.0 at nm^{-2} (▲). Horizontal dashed line corresponds to the result for brookite particles without doping and horizontal plain line to that of brookite particles sintered 24h at 500 °C.

Lower RhB concentration in the suspension after 2h of UV illumination means higher photocatalytic activity for tested nanoparticles. Note that the tests were conducted in iso-surface way, which means high quantity of material was used for the samples possessing low surface aera, e.g., those sintered with long time (see the Supporting Information, S7). The aim of this iso-surface study is to focus on the influence of surface coverage of brookite nanoparticles on the photocatalytic surface phenomenon. The results (Figure 8) show that the lanthanum-doping before sintering decreases the photocatalytic activity of brookite nanoparticles, which should be due to the surface impurity introduced by lanthanum adsorption onto the surface brookite. Interestingly, a short duration of sintering (4 h) enhances the photocatalytic activity to an extent that even surpasses the non-doped brookite, and this phenomenon is most pronounced for the sample with lanthanum surface coverage of 1 at nm^{-2}, followed by that of 0.7 at nm^{-2} and then 0.4 at nm^{-2}. One possible explanation is that 4 h of sintering improved the crystallinity of brookite nanoparticles and yielded little rutile for the sample with high lanthanum surface coverage (see the Supporting Information, S3). The brookite particles heated at 500 °C for 22 h display a poorer photocatalytic activity despite an improved crystalline quality (this sample consists of pure brookite particles with a particles size of 20 nm and a specific surface of 50 m^2.g^{-1}).that is why the crystalline quality is not the origin of the photocatalytic improvement. Moreover, longer duration of sintering began to decrease the photocatalytic activity, and sintering time equal to or more than 50 h even yielded negative effect comparing to non-doped brookite sintered for the same duration. This might be due to the formation of $La_4Ti_9O_{24}$ and large quantity of rutile upon prolonged heating treatment. Generally, with the same sintering time, brookite nanoparticles with higher lanthanum surface coverage showed always higher photocatalytic activity, As the photocatalytic activity tests were realized iso-surface way, the results confirm that higher lanthanum-doping improve the photocatalytic activity of brookite per surface area. Moreover, higher lanthanum-doping yielded always less loss of surface area of the brookite for the same sintering time at 800 °C (see the Supporting Information, S6). These two factors together suggest that higher lanthanum-doping should be positive for improving the photocatalytic efficiency of brookite.

4. CONCLUSION

The annealing behavior of brookite nanoparticles was fully investigated at various temperatures in terms of kinetic and phase transformation mechanisms. During the brookite to rutile phase transformation, the observation of anatase as transitory phase at high temperature conditions was associated to surface stabilization phenomena. The brookite thermal stability was also improved of almost 200 °C by the use of lanthanum as surface additive. Transformation mechanisms were proposed to account for the evolution of the different systems. This study demonstrates thus the importance of surface tailoring in the thermal stability of metastable polymorphs.

The surface doping performed in the present study allowed the formation of various combination of well crystallized polymorphs: anatase−rutile, brookite−rutile, and anatase−brookite rutile with various phase ratio. Such samples may be very useful in fundamental photocatalysis study to determine whether two TiO_2 polymorphs are really needed to optimize the photodegradation process. As for the direct impact of the surface doping, dispersed lanthanum ions on brookite particles improved its efficiency as photocatalyst as long as the mixed phase is not formed. The use of other surface doping that do not form mixed phase with titanium might give interesting results for longer sintering time

■ ASSOCIATED CONTENT

Ⓢ Supporting Information

Experimental and calculated adsorption isotherms of La (III) on brookite nanoparticles, X-ray diffraction patterns of as synthesized TiO_2 nanoparticles (a) and doped with different amounts of surface La atoms, amount of rutile formed with

time for La(III) doped brookite nanoparticles sintered at 800 °C and the corresponding TiO_2 nanoparticles size evolution with time, X-ray diffraction pattern of a brookite sample doped with La(III) at 1 at nm^{-2} after 5h30 of sintering at 900 °C, phase evolution of La doped brookite nanoparticles at 900 °C and BET surface aera evolution of La(III)-doped brookite nanoparticles sintered at 800 °C in function of sintering time for different La(III) surface coverage, are available in supplementary information. This material is available free of charge via the Internet at http://pubs.acs.org/.

AUTHOR INFORMATION

Corresponding Author

*Telephone: +33144271543. Fax: +33144271504. E-mail: olivier.durupthy@upmc.fr.

ACKNOWLEDGMENTS

This research work was supported by IFP Energies Nouvelles. The authors thank Isabelle Clemençon for the XRD measurements and Isabelle Muller for the thermogravimetric experiments.

REFERENCES

(1) Reisch, M. *Chem. Eng.* **2001**, *79*, 23.
(2) Sakai, A. *Fragrance J.* **2003**, *31*, 81.
(3) Fujishima, A.; Rao, T. N.; Tryk, D. A. *J. Photochem. Photobiol., C* **2000**, *1*, 1.
(4) Bonhôte, P.; Moser, J.-E.; Humphry-Baker, R.; Vlachopoulos, N.; Zakeeruddin, S. M.; Walder, L.; Grätzel, M. *J. Am. Chem. Soc.* **1999**, *121*, 1324.
(5) Lin, H.-M.; Keng, C.-H.; Tung, C.-Y. *Nanostruct. Mater.* **1997**, *9*, 747.
(6) Croce, F.; Appetecchi, G. B.; Persi, L.; Scrosati, B. *Nature* **1998**, *394*, 456.
(7) Baudrin, E.; Cassaignon, S.; Koesch, M.; Jolivet, J. P.; Dupont, L.; Tarascon, J. M. *Electrochem. Commun.* **2007**, *9*, 337.
(8) Magne, C.; Cassaignon, S.; Lancel, G.; Pauporte, T. *Chemphyschem* **2011**, *12*, 2461.
(9) Barbé, C. J.; Arendse, F.; Comte, P.; Jirousek, M.; Lenzmann, F.; Shklover, V.; Grätzel, M. *J. Am. Ceram. Soc.* **1997**, *80*, 3157.
(10) Kandiel, T. A.; Feldhoff, A.; Robben, L.; Dillert, R.; Bahnemann, D. W. *Chem. Mater.* **2010**, *22*, 2050.
(11) Murakami, N.; Kamai, T.-a.; Tsubota, T.; Ohno, T. *Catal. Commun.* **2009**, *10*, 963.
(12) Di Paola, A.; Bellardita, M.; Ceccato, R.; Palmisano, L.; Parrino, F. *J. Phys. Chem. C* **2009**, *113*, 15166.
(13) Di Paola, A.; Cufalo, G.; Addamo, M.; Ellardita, M. B.; Campostrini, R.; Ischia, M.; Ceccato, R.; Palmisano, L. *Colloids Surf., A* **2008**, *317*, 366.
(14) Bakardjieva, S.; Stengl, V.; Szatmary, L.; Subrt, J.; Lukac, J.; Murafa, N.; Niznansky, D.; Cizek, K.; Jirkovsky, J.; Petrova, N. *J. Mater. Chem.* **2006**, *16*, 1709.
(15) Yin, S.; Ihara, K.; Liu, B.; Wang, Y.; Li, R.; Sato, T. *Phys. Scr.* **2007**, *T129*, 268.
(16) Ardizzone, S.; Bianchi, C. L.; Cappelletti, G.; Gialanella, S.; Pirola, C.; Ragaini, V. *J. Phys. Chem. C* **2007**, *111*, 13222.
(17) Kominami, H.; Ishii, Y.; Kohno, M.; Konishi, S.; Kera, Y.; Ohtani, B. *Catal. Lett.* **2003**, *91*, 41.
(18) Ohtani, B.; Handa, J.; Nishimoto, S.; Kagiya, T. *Chem. Phys. Lett.* **1985**, *120*, 292.
(19) Bakardjieva, S.; Stengl, V.; Szatmary, L.; Subrt, J.; Lukac, J.; Murafa, N.; Niznansky, D.; Cizek, K.; Jirkovsky, J.; Petrova, N. *J. Mater. Chem.* **2006**, *16*, 1709.
(20) Perego, C.; Clemençon, I.; Rebours, B.; Revel, R.; Durupthy, O.; Cassaignon, S.; Jolivet, J.-P. *Mater. Res. Soc. Symp. Proc.* **2009**, *1146*, NN04.
(21) Chen, X.; Mao, S. S. *Chem. Rev.* **2007**, *107*, 2891.
(22) Durupthy, O.; Bill, J.; Aldinger, F. *Cryst. Growth Des.* **2007**, *7*, 2696.
(23) Liu, C.-E.; Rouet, A.; Sutrisno, H.; Puzenat, E.; Terrisse, H.; Brohan, L.; Richard-Plouet, M. *Chem. Mater.* **2008**, *20*, 4739.
(24) Pottier, A.; Chanéac, C.; Tronc, E.; Mazerolles, L.; Jolivet, J.-P. *J. Mater. Chem.* **2001**, *11*, 1116.
(25) Buonsanti, R.; Grillo, V.; Carlino, E.; Giannini, C.; Kipp, T.; Cingolani, R.; Cozzoli, P. D. *J. Am. Chem. Soc.* **2008**, *130*, 11223.
(26) Pottier, A.; Cassaignon, S.; Chanéac, C.; Villain, F.; Tronc, E.; Jolivet, J.-P. *J. Mater. Chem.* **2003**, *13*, 877.
(27) Cassaignon, S.; Koelsch, M.; Jolivet, J.-P. *J. Mater. Sci.* **2007**, *42*, 6689.
(28) Gribb, A. A.; Banfield, J. F. *Am. Mineral.* **1997**, *82*, 717.
(29) Hebrard, J. L.; Nortier, P.; Pijolat, M.; Soustelle, M. *J. Am. Ceram. Soc.* **1990**, *73*, 79.
(30) Hebrard, J. L.; Pijolat, M.; Soustelle, M. *Solid State Ionics* **1989**, *32-3*, 852.
(31) Kumar, K. N. P. *Scr. Metall. Mater.* **1995**, *32*, 873.
(32) Kumar, K. N. P.; Keizer, K.; Burggraaf, A. J.; Okubo, T.; Nagamoto, H.; Morooka, S. *Nature* **1992**, *358*, 48.
(33) Kumar, K. N. P.; Kumar, J.; Keizer, K. *J. Am. Ceram. Soc.* **1994**, *77*, 1396.
(34) Zhang, H. Z.; Banfield, J. F. *J. Mater. Res.* **2000**, *15*, 437.
(35) Penn, R. L.; Banfield, J. F. *Am. Mineral.* **1999**, *84*, 871.
(36) Zhang, H. Z.; Banfield, J. F. *Am. Mineral.* **1999**, *84*, 528.
(37) Zhang, H.; Banfield, J. F. *J. Mater. Chem.* **1998**, *8*, 2073.
(38) Zhang, H.; Banfield, J. F. *J. Phys. Chem. B* **2000**, *104*, 3481.
(39) Praserthdam, P.; Silveston, P. L.; Mekasuwandumrong, O.; Pavarajarn, V.; Phungphadung, J.; Somrang, P. *Cryst. Growth Des.* **2004**, *4*, 39.
(40) Perego, C.; Revel, R.; Durupthy, O.; Cassaignon, S.; Jolivet, J.-P. *Solid State Sci.* **2010**, *12*, 989.
(41) Reidy, D. J.; Holmes, J. D.; Morris, M. A. *J. Eur. Ceram. Soc.* **2006**, *26*, 1527.
(42) Zhang, H. Z.; Banfield, J. F. *American Mineralogist* **1999**, *84*, 528.
(43) Zhang, J.; Li, M. J.; Feng, Z. C.; Chen, J.; Li, C. *J. Phys. Chem. B* **2006**, *110*, 927.
(44) Gopalan, R.; Lin, Y. S. *Ind. Eng. Chem. Res.* **1995**, *34*, 1189.
(45) Ruiz, A. M.; Cornet, A.; Morante, J. R. *Sens. Actuators, B* **2004**, *100*, 256.
(46) Choi, J.; Park, H.; Hoffmann, M. R. *J. Phys. Chem. C* **2010**, *114*, 783.
(47) Rao, C. N.; Yoganarasimhan, S. R.; Faeth, P. A. *Trans. Faraday Soc.* **1961**, *57*, 504.
(48) Li, J. G.; Ishigaki, T. *Acta Mater.* **2004**, *52*, 5143.
(49) Huberty, J.; Xu, H. *J. Solid State Chem.* **2008**, *181*, 508.
(50) Kominami, H.; Kohno, M.; Kera, Y. *J. Mater. Chem.* **2000**, *10*, 1151.
(51) Xu, Q.; Zhang, J.; Feng, Z.; Ma, Y.; Wang, X.; Li, C. *Chem—Asian J.* **2010**, *5*, 2158.
(52) Morishima, Y.; Kobayashi, M.; Petrykin, V.; Kakihana, M.; Tomita, K. *J. Ceramic. Soc. Jpn.* **2007**, *115*, 826.
(53) Lee, J. H.; Yang, Y. S. *J. Mater. Sci.* **2006**, *41*, 557.
(54) Liu, C.-E.; Rouet, A.; Sutrisno, H.; Puzenat, E.; Terrisse, H.; Brohan, L.; Richard-Plouett, M. *Chem. Mater.* **2008**, *20*, 4739.
(55) Bellardita, M.; Di Paola, A.; Palmisano, L.; Parrino, F.; Buscarino, G.; Amadelli, R. *Appl. Catal., B* **2011**, *104*, 291.
(56) Di Paola, A.; Bellardita, M.; Marci, G.; Palmisano, L.; Parrino, F.; Amadelli, R. *Catal. Today* **2011**, *161*, 35.
(57) Kosmulski, M. *Adv. Colloid Interface Sci.* **2002**, *99*, 255.
(58) Savvin, S. B.; Shvoeva, O. P.; Dedkova, V. P. *J. Anal. Chem.* **2005**, *60*, 330.
(59) Tompsett, G. A.; Bowmaker, G. A.; Cooney, R. P.; Metson, J. B.; Rodgers, K. A.; Seakins, J. M. *J. Raman Spectrosc.* **1995**, *26*, 57.
(60) Ohsaka, T.; Izumi, F.; Fujiki, Y. *J. Raman Spectrosc.* **1978**, *7*, 321.
(61) Liqiang, J.; Xiaojun, S.; Baifu, X.; Baiqi, W.; Weimin, C.; Honggang, F. *J. Solid State Chem.* **2004**, *177*, 3375.
(62) Shannon, R. D.; Pask, J. A. *J. Am. Ceram. Soc.* **1965**, *48*, 391.

(63) Banfield, J. F.; Bischoff, B. L.; Anderson, M. A. *Chem. Geol.* **1993**, *110*, 211.
(64) Zhang, H. Z.; Banfield, J. F. *J. Mater. Res.* **2000**, *15*, 437.
(65) Sibu, C. P.; Kumar, S. R.; Mukundan, P.; Warrier, K. G. K. *Chem. Mater.* **2002**, *14*, 2876.
(66) Nguyen-Phan, T. D.; Song, M. B.; Kim, E. J.; Shin, E. W. *Microporous Mesoporous Mater.* **2009**, *119*, 290.
(67) Reddy, B. M.; Sreekanth, P. M.; Reddy, E. P.; Yamada, Y.; Xu, Q.; Sakurai, H.; Kobayashi, T. *J. Phys. Chem. B* **2002**, *106*, 5695.
(68) Ruiz, A. M.; Cornet, A.; Morante, J. R. *Sens. Actuators, B* **2005**, *111-112*, 7.
(69) Ma, Y.; Zhang, J.; Tian, B.; Chen, F.; Wang, L. *J. Hazard. Mater.* **2010**, *182*, 386.
(70) Lu, K. *Mater. Sci. Eng., B* **1996**, *16*, 161.
(71) Rao , C. N. R.; Rao , K. J. *Phase Transitions in Solids: An Approach to the Study of the Chemistry and Physics of Solid*; McGraw-Hill: New York, 1978.
(72) Suzuki, A.; Kotera, Y. *Bull. Chem. Soc. Jpn.* **1962**, *35*, 1353.
(73) Banfield, J. F.; Bischoff, B. L.; Anderson, M. A. *Chem. Geol.* **1993**, *110*, 211.
(74) Czanderna, A. W.; Rao, C. N. R.; Honig, J. M. *Trans. Faraday Soc.* **1958**, *54*, 1069.
(75) Mackenzie, K. J. D. *Trans. J. Br. Ceram. Soc.* **1975**, *74*, 77.
(76) Heald, E. F.; Weiss, C. W. *Am. Mineral.* **1972**, *57*, 10.
(77) Suzuki, A.; Tukuda, R. *Bull. Chem. Soc. Jpn.* **1969**, *42*, 1853.
(78) Hishita, S.; Mutoh, I.; Koumoto, K.; Yanagida, H. *Ceram. Int.* **1983**, *9*, 61.
(79) Suzuki, A.; Tukuda, R. *Bull. Chem. Soc. Jpn.* **1969**, *42*, 1853.
(80) Kumar, K. N. P.; Keizer, K.; Burggraaf, A. J. *J. Mater. Chem.* **1993**, *3*, 1141.